Prediction of Au-Associated Minerals in Eastern Thailand Based on Stream Sediment Geochemical Data Analysis by S-A Multifractal Model

Oraphan Yaisamut [1,2], Shuyun Xie [1,*], Punya Charusiri [2], Jianbiao Dong [1] and Weiji Wen [1]

1 State Key Laboratory of Geological Processes and Mineral Resources (GPMR), Faculty of Earth Sciences, China University of Geosciences, Wuhan 430074, China; noon-oraphan@hotmail.com (O.Y.); 15849571958@163.com (J.D.); cugwenweiji@163.com (W.W.)
2 Department of Mineral Resources, Ministry of Natural Resources and Environment, 75/10 Rama VI Road, Ratchathewi, Bangkok 10400, Thailand; punya.c@chula.ac.th
* Correspondence: tinaxie@cug.edu.cn

Abstract: Conducted within the scope of geochemical exploration in eastern Thailand, this study aims to detect geochemical anomalies and potential mineral deposits. The objective was to interpret intricate spatial dispersion patterns and concentration levels of deposit pathfinder elements, specifically arsenic (As), copper (Cu), and zinc (Zn), using a comprehensive array of stream sediment geochemistry data. Methodologies involved integrating multifractal properties and traditional statistics, facilitated by the GeoDAS and ArcGIS platforms as instrumental analytical tools. In total, 5376 stream sediment samples were collected and evaluated, leading to the development of an in-depth geochemical map. The results indicated distinct geological units marked by substantially elevated average values of the aforementioned elements. Identification of geochemical anomalies was achieved through the spatial distribution method and the subsequent application of the spectrum-area (S-A) multifractal model. An intriguing link was found between high As concentrations and gold deposits in the area, suggesting As as a viable pathfinder element for gold mineralization. The anomaly maps, generated from the stream sediment data, spotlighted potential zones of interest, offering valuable guidance for future mineral exploration and geological inquiries. Nonetheless, it is vital to recognize that the increased values noted in these maps may be influenced by regional geological factors, emphasizing the necessity for a diverse set of analytical methods for accurate interpretation. This study's significance lies in its pioneering use of the S-A multifractal model in geochemical data analysis. This innovative approach has deepened our comprehension of geochemical dispersion patterns and improved the precision of mineral exploration.

Keywords: eastern Thailand; geochemical exploration; pathfinder elements; stream sediment; spectrum-area (S-A) multifractal model; pathfinder elements

1. Introduction

Geochemical exploration is essential in identifying undiscovered mineral deposits [1–4]. It uses multiple methods to analyze data, revealing the geographic patterns of geochemical markers, identifying related elements, and detecting geochemical anomalies due to mineralization processes [5–7]. To investigate these processes, a regional geochemical survey is needed. Regional geochemical surveys are crucial in both environmental and mineral exploration studies [8–10]. They provide baseline data about the distribution and abundance of elements and compounds in a region, serving as a reference point for future studies. In environmental studies, these surveys help assess the environmental quality, monitor changes over time, and evaluate the effectiveness of mitigation measures [11]. In mineral exploration, they identify areas with economically valuable minerals by creating geochemical maps that highlight anomalous zones [12]. Overall, regional geochemical surveys provide

essential information for understanding the environment, identifying mineral deposits, refining geological models, and making informed decisions about land use. These surveys also contribute to geologic mapping efforts and aid in land use planning and resource management. Geochemical anomalies have become more significant in the process of regional mineral prediction in recent decades. Geochemical element distribution patterns at the surface are the result of several primary and secondary geological processes [13,14].

In recent decades, there have been significant advancements in the processing of geochemical data, revolutionizing our understanding of Earth's processes, environmental changes, and resource assessments. This process involves several crucial steps, including data quality control, normalization, transformation, statistical analysis, visualization, geo-statistics, data integration, and computational modeling. Through these methods, data reliability is ensured, enabling effective comparison, interpretation, exploration of relationships and trends, visualization of results, analysis of spatial patterns, integration of data from multiple sources, and simulation of geochemical processes. Researchers have extensively studied state-of-the-art methods for processing geochemical exploration data over the past several decades [15]. The field has witnessed the introduction of various advanced mathematical and statistical techniques to analyze geochemical data exploration [16,17]. These methods have transitioned from traditional and multivariate statistics to more sophisticated approaches, such as fractal/multifractal models [18,19] and machine learning/deep learning [7]. Geochemistry relies on conventional statistical methods to decipher and interpret the properties of geochemical elements. Traditional statistics, such as classical statistics, have been instrumental in identifying geochemical anomalies using various methods [20–24]. Several successful traditional techniques have been applied to analyze geochemical data. While traditional methods, including multivariate statistics, are commonly employed to define thresholds and distinguish subpopulations [23,25], they often overlook the spatial information and autocorrelation structure present in geochemical data. These methods can be seen as non-spatial statistical tools. To address this limitation, spatial statistical methods, such as the moving average technique, have been developed to incorporate the spatial aspect of geochemical data analysis.

Univariate statistics have become standard in understanding the distribution attributes of geochemical elements, assisting in pinpointing pathfinder elements, and interpreting their dynamics. Meanwhile, spatial data analysis methods, such as geo-statistics [26] and fractal analysis [27], have gained popularity as frequency-space-based approaches. These methods, often augmented with Geographic Information Systems (GIS), facilitate the modeling and quantification of spatial discrepancies in geochemical data. Important concepts in non-linear and complexity sciences, fractal and multifractal models have found recognition in geosciences [18,26–30] and have been developed for analyzing geochemical data. These models serve as potent tools in identifying geochemical anomalies and setting geochemical baselines in diverse studies, such as concentration-area (C-A) model [31,32], spectrum-area (S-A) model [33–35], and singularity analysis [3,36–38].

In this study, classical statistics and multifractal properties are used in analyzing stream sediment geochemistry data for the region. The aim is to distinguish local anomalies from the complex geological background and summarize them to generate a geochemical map. The map provides insights into the concentration values of deposit pathfinder elements, which have multiple chemical element populations and complex spatial dispersion patterns. The primary focus lies in applying advanced GIS techniques [19,39], specifically utilizing the GeoDAS and ArcGIS platforms, to delineate promising areas with anomalies of pathfinder elements [40–47] associated with gold (As, Cu, and Zn) in eastern Thailand.

2. Geological Settings

The study area is located in the eastern region of Thailand. As illustrated in Figure 1, eastern Thailand has a varied topography, with numerous low-relief areas interrupted by linear hills and ridges. Cenozoic strike-slip faults have influenced these landforms to trend NW–SE [48]. The area is characterized by a series of sedimentary basins, volcanic rocks,

and granitic intrusions that record a complex tectonic history [49] involving the Sibumasu terrane, Chanthaburi terrane, and Indochina terrane [50–52]. During the Permo–Triassic period, a volcanic arc system [53] existed in the Chanthaburi terrane, which is characterized by its location, sandwiched between the Indochina and Sibumasu continental blocks.
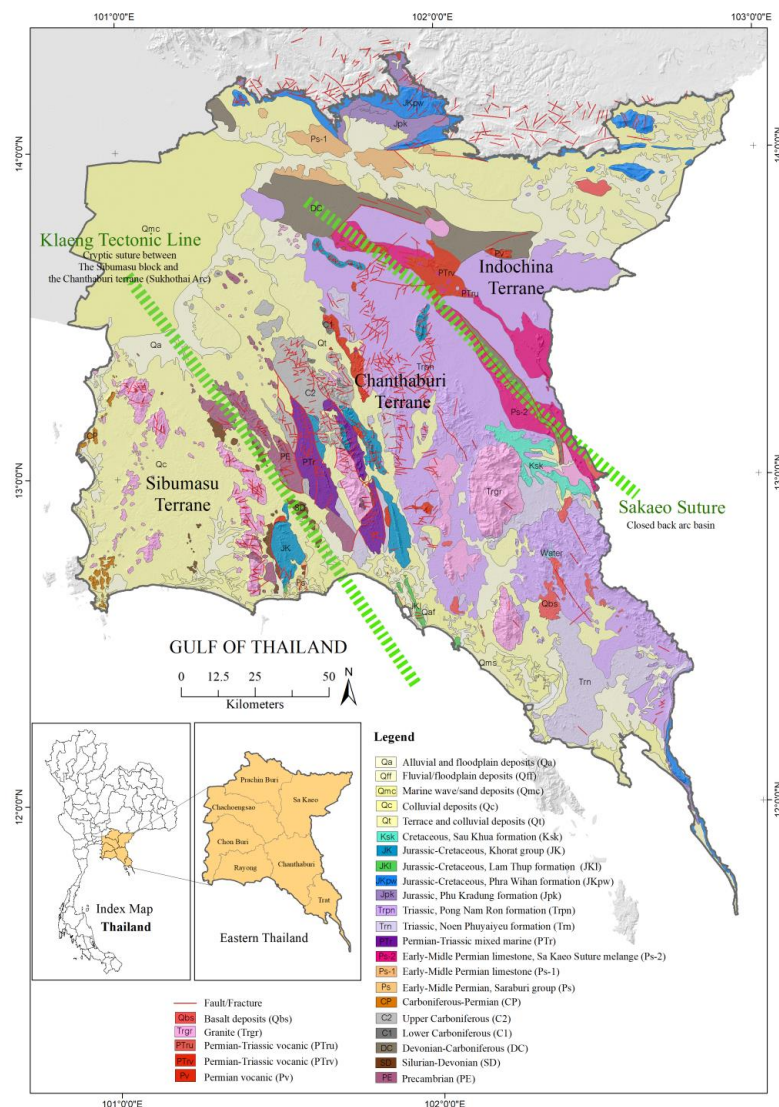

Figure 1. Geological map of the study area in eastern Thailand, showing major rock units with the Sakaeo back-arc suture, which encircles the Chanthaburi terrene, and the Klaeng tectonic line, which separates the Chanthaburi and Sibumasu blocks (partly adapted from DMR, 1999).

The Chanthaburi terrane is a distinct fragment of the Sukhothai Arc, as identified by Sone and Metcalfe (2008) [54]. Noted for its I-type granitic plutons and radiometrically linked to the Triassic–Jurassic eras, the terrane is defined by its boundaries with the In-dochina and Sibumasu blocks, outlined by the Sa Kaeo Suture [55] and the Klaeng tectonic line, respectively. This terrane is home to a diverse range of marine sediments from the Carboniferous and late Permian–Triassic periods, all with rich fossil records, as well as deep-water Triassic sediments and younger Mesozoic continental sediments [54,56–58]. Additionally, the Klaeng tectonic line, a significant fault, speaks to a past of tectonic activity and collision between the Sibumasu block and the southern Sukhothai Arc. This fault line exhibits several geological characteristics, including mylonitic gneisses and low-grade metamorphic rocks [59].

The Chanthaburi terrane also includes various sedimentary deposits. Carboniferous sediments found in three major limestone hills exhibit similarities with Early Carboniferous fauna found in other parts of Thailand and Laos. The terrane also houses late Permian–Triassic sediments, particularly those discovered in the Sukpaiwan Formation. These deposits contain a diverse range of fossils that establish a stratigraphic continuity from the late Permian to the Middle Triassic [58,59]. The terrane also contains Triassic sediments from deeper marine environments, as represented by the Pong Nam Ron Formation and the Noen Po Formation, inclusive of cherts from the Late and Middle Triassic [60–62]. Furthermore, it hosts younger Mesozoic continental sediments, conspicuous in southeast Thailand, which have been connected to the Jurassic–Cretaceous Khorat Group [63–67].

The base of the granitic belt in Thailand is composed of the Western, Central, and Eastern belts [68], as shown in Figure 2. Eastern Thailand incorporates the Triassic granite found in the Central belt, referred to as the Sibumasu terrane. This type of terrane is classified as S-type granite. Additionally, the Chanthaburi terrane, classified as I-type granite, is known as the Triassic granite in the Eastern belt. Notably, gold deposits are related to the I-type granite found in the Chanthaburi Terrane [60,69], while heavy minerals are associated with the S-type granite [69–71].
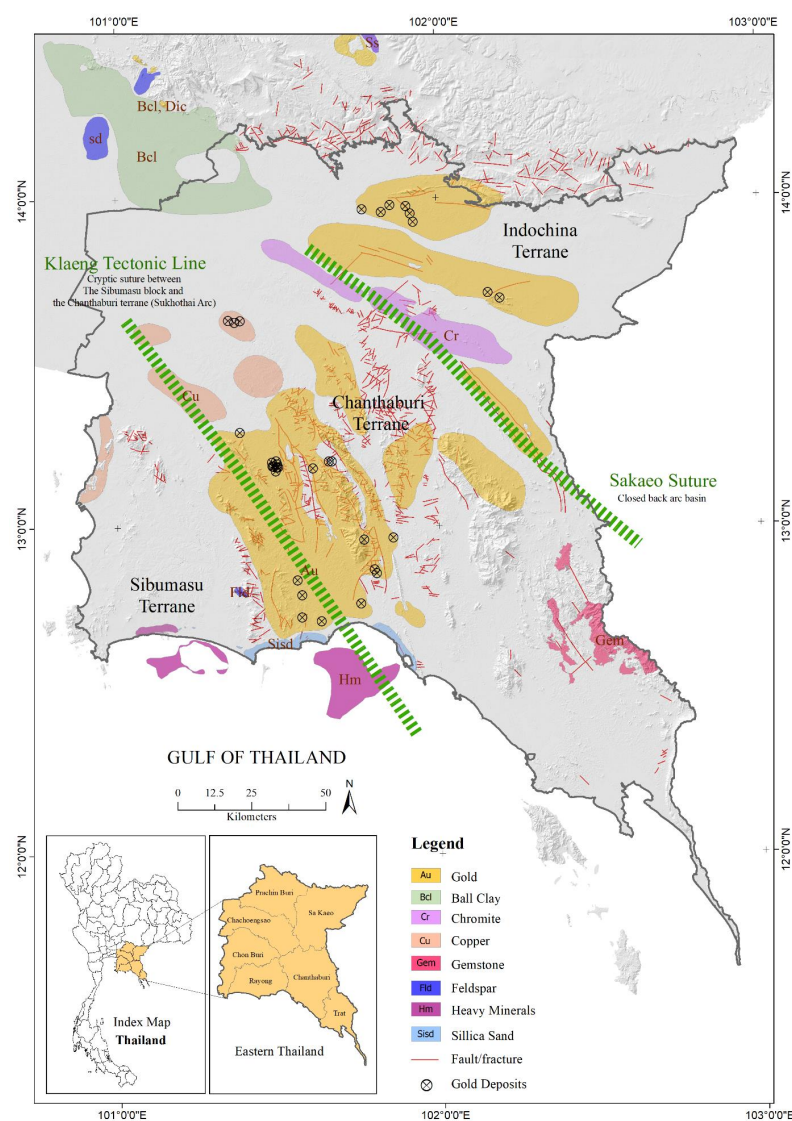

Figure 2. Mineral deposits in eastern Thailand, located in the Sibumasu Terrane, Chanthaburi Terrane, and Indochina Terrane (partly adapted from DMR, 2006).

This area has several significant mineral deposits, which align with the Central metallogenic province [69]. Some base metals, including chromium, tungsten, gold, silver, and copper [72], are primarily found in association with Permo–Triassic volcanic rocks and Triassic granitic intrusions, which are believed to have been emplaced during the collision of the Indian and Eurasian Plates [73]. Additionally, gemstones and silica sand deposits are present in the east corner of the country, and recent exploration has also shown that gold potential is also high [74]. Finally, in the Gulf of Thailand, numerous Tertiary basins are the source of natural gas and petroleum (Figure 2).

3. Methodology

3.1. Geochemical Data

The total collected samples were 5376 stream sediment samples (Figure 3) from stream systems in eastern Thailand, with a density of a sample per 5 km^2. The data were collected under the Department of Mineral Resources in Thailand (DMR), covering 34,380 km^2 of territory, with multi-element analyses of 12 elements, with elements As (arsenic), Ba (barium), Co (cobalt), Cr (chromium), Cu (copper), Fe (iron), Mg (magnesium), Mn (manganese), Ni (nickel), Pb (lead), V (vanadium), and Zn (zinc). The samples were collected from active stream sediment [75,76] consisting of clay to sand-sized particles along a 30–50 m stretch of the stream. The sediment sample was prepared by sieving it to provide 2–3 kg of the 80-mesh fraction for analysis. Large samples were necessary to minimize the "nugget effect", which refers to small-scale variations in the element concentration within a sample. A multi-element analytical methodology and a unified data quality monitoring of the procedure were used to analyze the sediment samples. Each sample was digested in a modified aqua regia solution and analyzed by using a Parkin Elmer Optima 5300 DV spectrometer (Norwalk, CT, USA) via inductively coupled plasma optical emission spectrometry (ICP-OES) [77] for 12 elements, with numbers in parentheses denoting detection limits: As (2 ppm), Ba (3 ppm), Co (1 ppm), Cr (1 ppm), Cu (2 ppm), Fe (30 ppm), Mg (50 ppm), Mn (1 ppm), Ni (1 ppm), Pb (4 ppm), V (1 ppm), and Zn (7 ppm).

3.2. Descriptive Statistics

Various measures were used in the statistical analysis, including the maximum value (Max), minimum value (Min), average value, mean value (X), standard deviation (SD), and coefficient of variation (CV). These measures are essential for understanding the behavior of geochemical elements in the study area and comparing datasets. A high SD indicates that the data points are widely spread out from the mean, while a low SD indicates that the data points are tightly clustered around the mean. The SD is useful for comparing the variability of two or more datasets or determining whether a particular data point is statistically significant or unusual relative to the rest of the data [78]. Elements' concentrations within these samples were considered because these elements represent the mineralization composition in this region [33].

3.3. The Spectrum-Area (S-A) Multifractal Model

The S-A model was developed by Cheng et al. in 1999 and 2012, and is a helpful method for identifying mixed geochemical patterns in complex geological environments. This model separates geochemical anomalies from the background based on distinct anisotropic scaling properties in the frequency domain, which has been a powerful tool to decompose mixed geochemical patterns [31,79]. The S-A model employs spectral analysis. The spatial distribution of orebodies can be better understood using these novel models. To create a new method that can not only distinguish between anomalies and background but also reveal information on the anisotropic scale invariance of geochemical patterns, Cao and Cheng (2012) merged the S-A model and generalized scale invariance using a power-law function that describes the relationship between the spectral energy density value (S) and the area in units (A) of the wave number, with a threshold $\geq$ S, and with spectral energy density values above S on the power density plane [80].

The equation of the S-A model is:

$$A \ (\geq S) \propto S^{-2d/\beta} \tag{1}$$

where S is the spectral energy density value, A ($\geq$S) is the area with a threshold larger than or equal to S, β is an anisotropic scaling exponent, d is a parameter representing the degree of the overall concentration, and $\propto$ denotes proportionality.

The following are the steps for applying the S-A model: (1) Turn the gridded data into the frequency domain by using the fast Fourier transformation, (2) establish the power spectrum of the data, (3) compute A(S) to find the region with a threshold greater than or equal to S, and (4) make an S-A log–log plot. (5) Before creating the filter, choose the S threshold value (breakpoints in the log–log plot). (6) Then, an inverse fast Fourier technique is used to transform the resulting power spectra. In step 5, there can be two filters: the low- and high-pass filters result in the creation of two maps, the first of which is the anomaly map and the second of which is the background map.
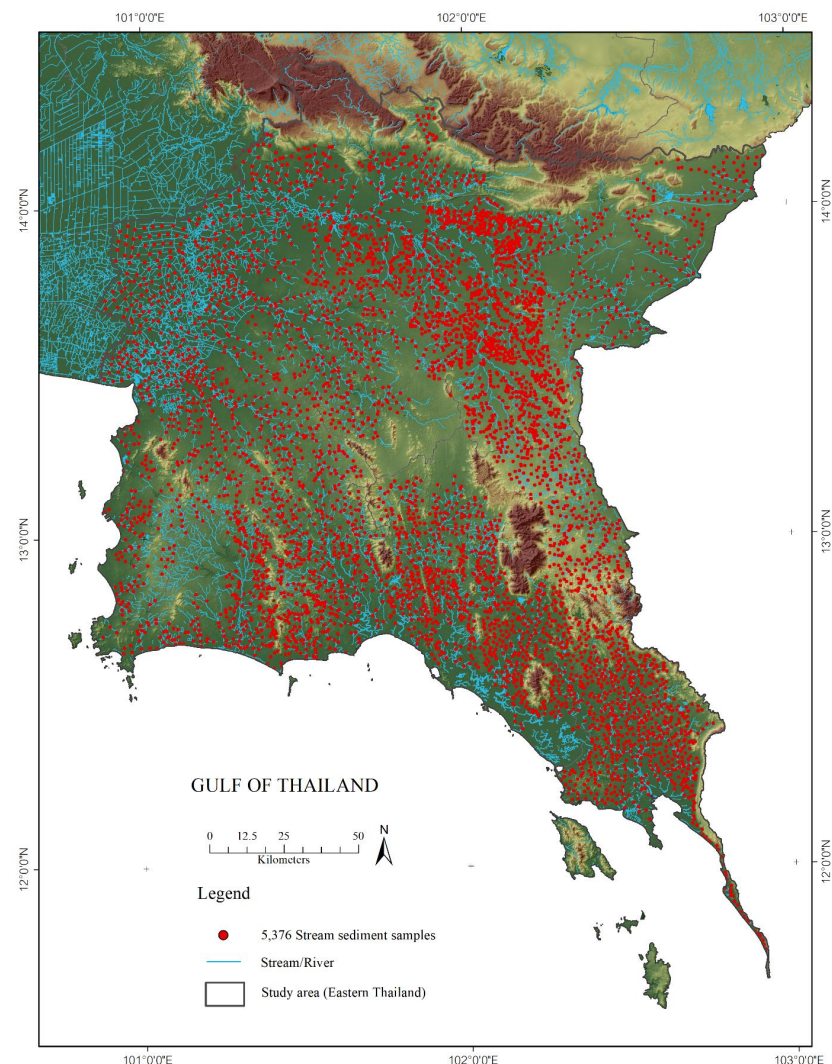

Figure 3. Location of 5376 stream sediment samples with a density of a sample per 5 km^2, covering 34,380 km^2 of territory, with multi-element analyses of 12 elements, with elements As, Ba, Co, Cr, Cu, Fe, Mg, Mn, Ni, Pb, V, and Zn.

4. Results and Discussion

4.1. Descriptive Statistics

Descriptive statistics of pathfinder elements for gold deposits (As, Cu, and Zn) are shown in Table 1. The high coefficient of variation (CV) values for As, Cu, and Zn concentrations (183.61%, 159.75%, and 302.55%, respectively) indicate the extremely variable concentrations of these elements. The CV values were used for the description of global variability. These statistical findings suggest that eastern Thailand comprises a variety of geochemical environments and has undergone a variety of different geological events over geological time, that resulted in complex ore-forming processes. Some of the values, particularly the incredibly high values, might fit fractal or multifractal distributions. Then, based on SPSS, the fractal distribution histograms and a quantile–quantile (Q-Q) plot were used for visualizing the distribution of geochemical data. For the distribution histograms (log 10), three elements, As, Cu, and Zn, had high skewness values, indicating that these data were not normally distributed and contained outliers, showing clearly positively skewed distributions, indicating that some data points in this dataset were inclined toward the distribution with high values. The skewness of As, Cu, and Zn was 16.74, 31.25, and 6.86, respectively. Based on their Q-Q plots, they were not normally distributed [2] because the point dots departed from the normal straight lines (Figure 4).

Table 1. Descriptive statistics for elements of 5376 stream sediment geochemical data points of As, Cu, and Zn, used in eastern Thailand.

Elements	N	Max [1]	Min [1]	X [1]	SD [1]	CV%	Skewness
As	5376	534.50	<DL [2]	7.05	12.95	183.61	16.74
Cu	5376	1760.00	<DL	20.26	32.36	159.75	31.25
Zn	5376	6657.00	<DL	46.45	140.53	302.55	6.86

[1] The units of elements are ppm. [2] DL = Detection limits (As = 2 ppm, Cu = 2 ppm, Zn = 7 ppm).

(**a**)

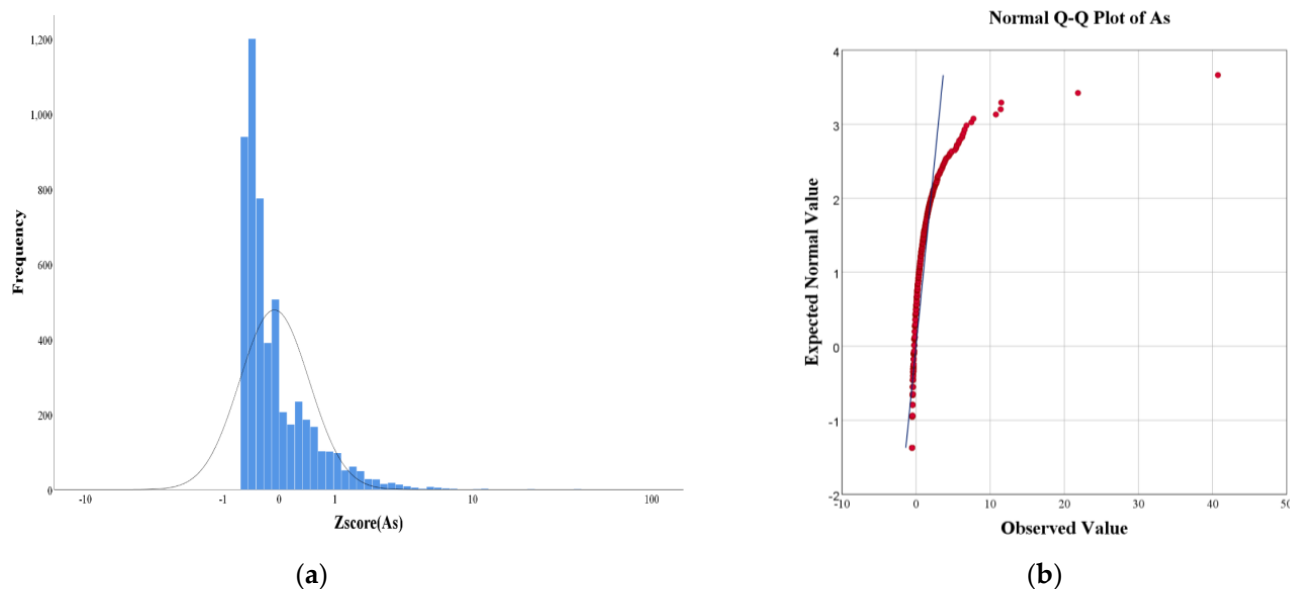
(**b**)

Figure 4. *Cont.*

(c)
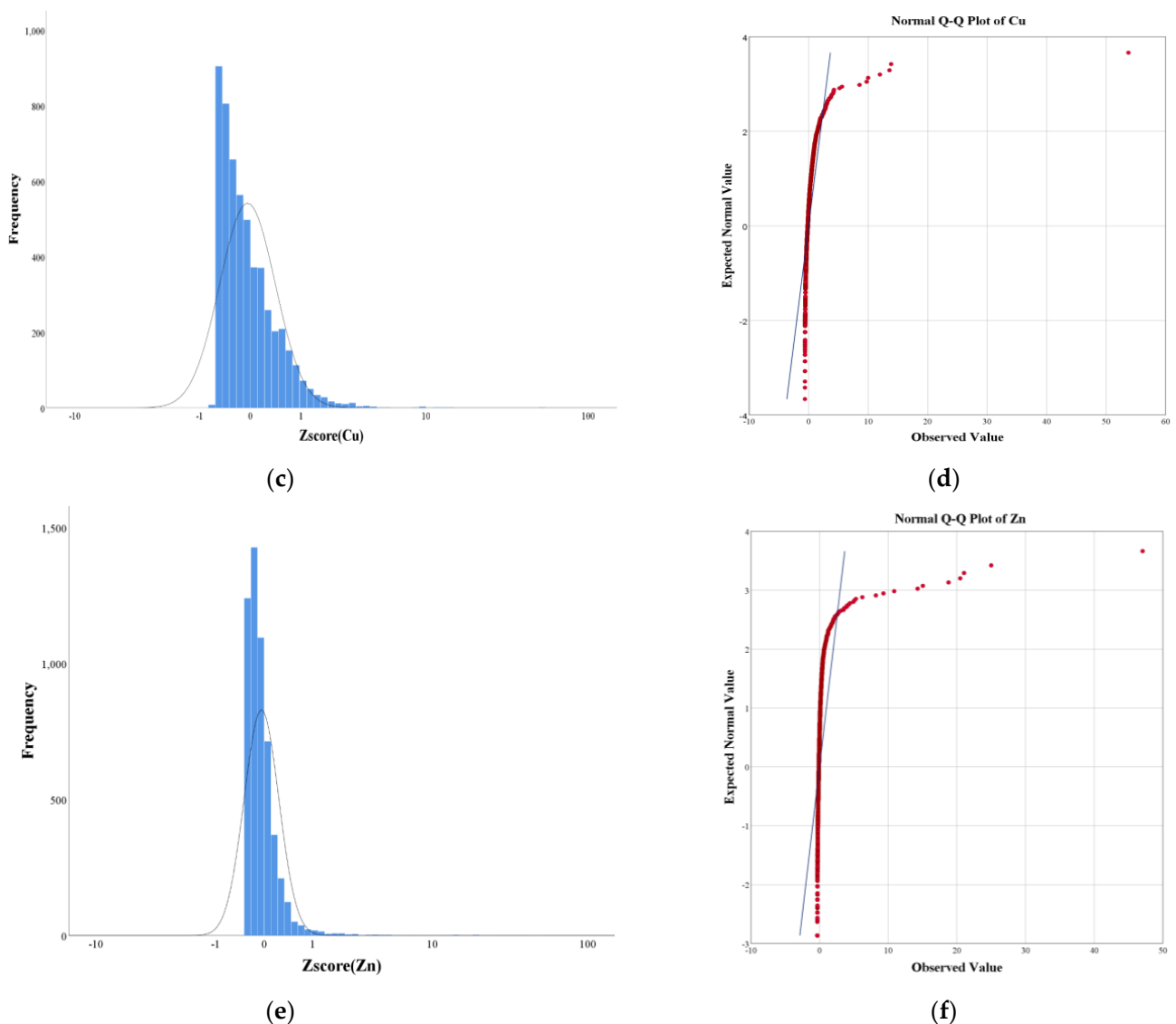

(d)

(e)

(f)

Figure 4. Distribution histograms of As (**a**), Cu (**c**), and Zn (**e**) concentrations in the stream sediments have high skewness values, indicating non-normal distribution, outliers, and positive skewness. Q−Q plots of As (**b**), Cu (**d**), and Zn (**f**) indicate that they were not normally distributed.

4.2. Spatial Distribution of As, Cu, and Zn

Anomaly areas with high stream sediment As concentrations (>24.00 ppm, 95th percentile), represented by red shading, are delineated in Figure 5. In total, anomalies can be divided into three zones in NW–SE orientations. Zone I is located in the western part of the study area of the Sibumasu Terrane, composed of granitic rocks (Trgr) and the sedimentary rocks of Carboniferous–Permian (CP), covered mostly by Quaternary sediment (Q). Zone II may be associated with the granitic rocks' (Trgr) intrusion and is located in the middle part of the study area of the Chanthaburi Terrane, composed of the Precambrian sedimentary rocks (PE), Upper Carboniferous (C2), Permian–Triassic mixed marine (PTr), Triassic Noen Phuyaiyeu Formation (Trn), and Jurassic–Cretaceous Khorat Group (JK). Zone III is located in the eastern part of the study area, covering the Chanthaburi Terrane and the Indochina Terrane, which was emplaced by the granitic rocks (Trgr), Permian–Triassic volcanic rock (PTrv), and the sedimentary rocks, Early–Middle Permian Limestone Sa Kaeo Suture Melange (Ps-2).

Strong stream sediment anomaly zones in Figure 5, with their Cu concentrations (>50.50 ppm, 95th percentile), are indicated by red shading. Anomalies can be split into three zones overall in NW–SE orientations. Zone I is located in the western part of Sibumasu Terrane and is associated with Granitic rocks (Trgr) and the sedimentary rocks Carboniferous–Permian (CP). Zone II is located in the middle of the study area of Chanthaburi Terrane and is associated with the Precambrian sedimentary rocks (PE). Zone III is located in the eastern part of the study area of the Indochina Terrane, associated with the intrusive rocks, Permian volcanic (Pv).

Anomaly regions with strong stream sediment Zn (Figure 5) contents (>100 ppm, 95th percentile) are indicated by red stippling. In total, the anomalies can be divided into two zones. Zone I in NW–SE orientations is located in the western part of Sibumasu Terrane and is associated with granitic rocks (Trgr), as well as the Precambrian sedimentary rocks (PE) and Carboniferous–Permian (CP). Zone II is located in the middle of the study area of Chanthaburi Terrane, covered mostly by Quaternary sediment (Q).

The elements were statistically distributed across the geological units, including Quaternary (Q), Cretaceous Sau Khua Formation (Ksk), Jurassic–Cretaceous Khorat Group (JK), Jurassic–Cretaceous Lam Thup Formation (JKl), Jurassic–Cretaceous Phra Wihan Formation (JKpw), Jurassic Phu Kradung Formation (Jpk), Triassic Pong Nam Ron Formation (Trpn), Triassic Noen Phuyaiyeu Formation (Trn), Permian–Triassic mixed marine (PTr), Early–Middle Permian Limestone Sa Kaeo Suture Melange (Ps-2), Early–Middle Permian Limestone (Ps-1), Early–Middle Permian Saraburi Group [55], Carboniferous–Permian (CP), Upper Carboniferous (C2), Lower Carboniferous (C1), Devonian–Carboniferous (DC), Silurian–Devonian (SD), Precambrian (PE), basalt deposits (Qbs), granitic rock (Trgr), Permian–Triassic volcanic (PTru, PTrv), and Permian volcanic (Pv) [81]. Table 2 summarizes these units, and their distribution characteristics were analyzed to determine the distribution of elements.
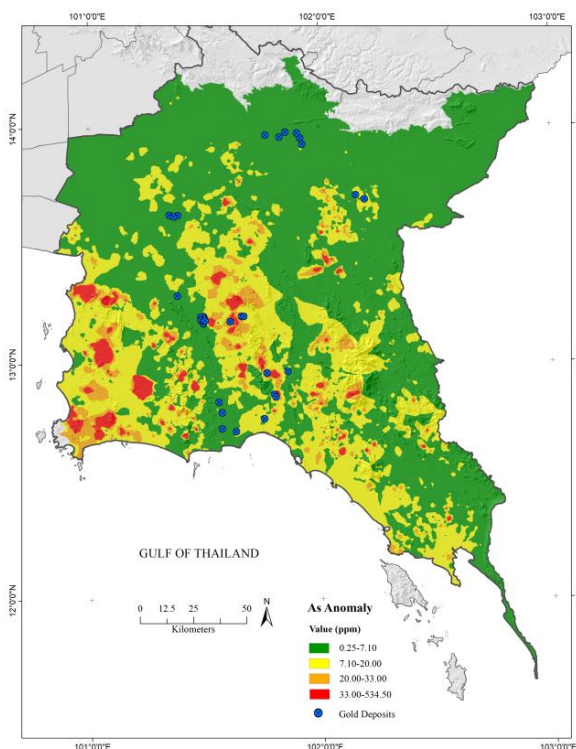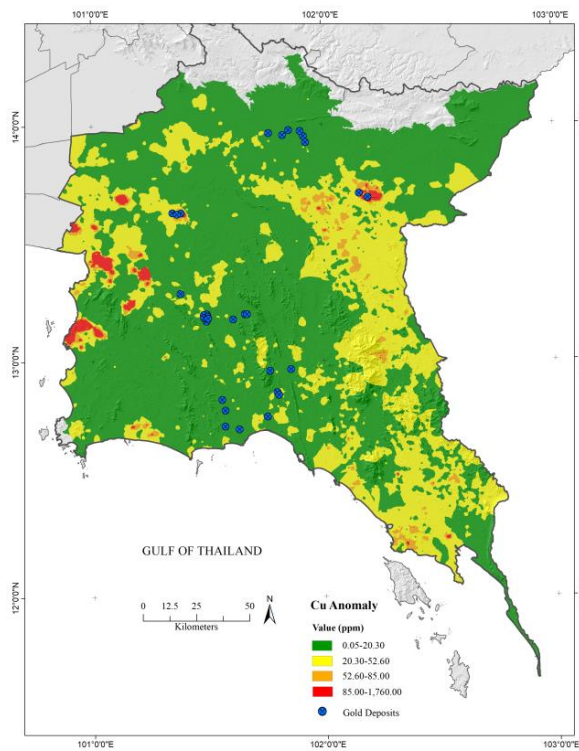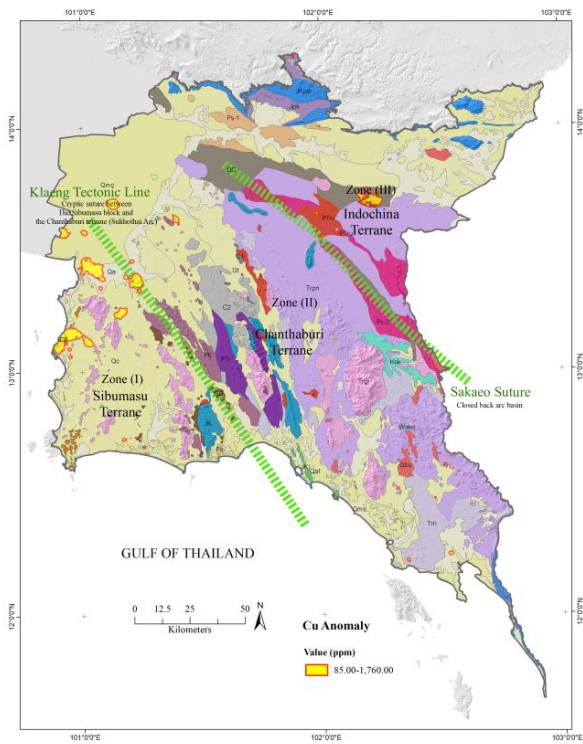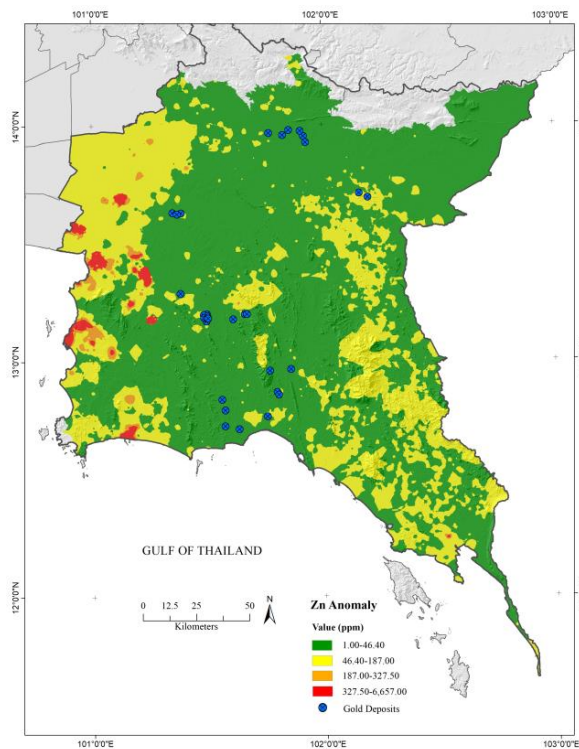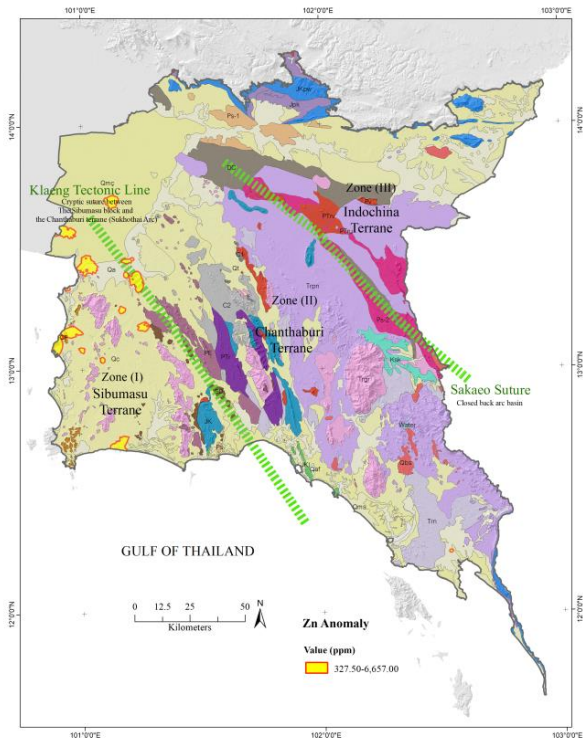

(a)
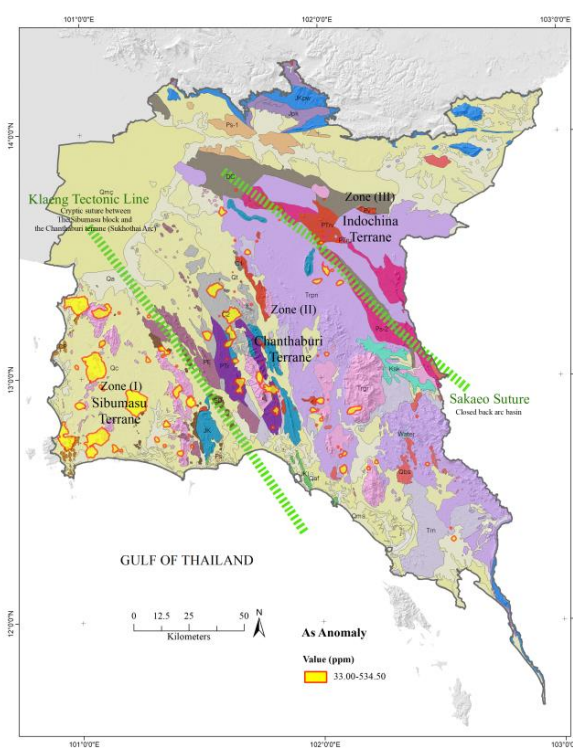
(b)

Figure 5. *Cont.*

(**c**)

(**d**)

(**e**)

(**f**)

Figure 5. Raster maps were created from the total concentration values of As (**a**), Cu (**c**), and Zn (**e**) in 5376 samples. The color classes are based on the following percentiles of raw data: 50, 75, 90, and 95 content. Stream sediment values show 95th percentile concentrations of As (**b**), Cu (**d**), and Zn (**f**). Anomalies represented by red shading overlayed with the geologic map can be divided into the zones of anomalies in NW–SE orientations.

Table 2. Statistical parameters for As, Cu, and Zn (ppm) of the geological unit in eastern Thailand.

Geological Unit	Samples (N)	Elements								
		As			Cu			Zn		
		X	SD	CV	X	SD	CV	X	SD	CV
Total	5376	7.05	12.95	1.84	20.26	32.36	1.60	46.45	140.53	3.03
Q	2447	7.40	15.91	2.15	16.55	43.47	2.63	57.38	206.49	3.60
Ksk	32	2.83	4.38	1.55	31.12	12.62	0.41	47.47	11.23	0.24
Jk	132	5.94	10.82	1.82	6.61	6.24	0.94	13.83	12.16	0.88
Jkl	5	6.00	6.27	1.04	10.14	8.07	0.80	11.60	8.73	0.75
JKpw	49	2.07	1.21	0.58	6.14	4.38	0.71	23.87	14.83	0.62
Jpk	60	5.94	10.82	1.82	6.61	6.24	0.94	13.83	12.16	0.88
Trpn	1207	6.16	8.97	1.46	22.37	12.45	0.56	38.89	18.35	0.47
Trn	313	6.73	6.86	1.02	26.10	15.82	0.61	40.16	21.93	0.55
PTr	100	19.74	17.35	0.88	17.32	7.69	0.44	32.79	17.32	0.53
Ps-2	201	19.74	17.35	0.88	17.32	7.69	0.44	32.79	17.32	0.53
Ps-1	37	3.50	6.21	1.78	15.30	12.10	0.79	27.05	18.32	0.68
Ps	3	5.11	2.80	0.55	22.29	18.69	0.84	22.48	16.95	0.75
C2	67	22.33	14.80	0.66	15.40	6.35	0.41	39.62	31.68	0.80
DC	291	4.43	6.17	1.39	30.39	29.64	0.98	33.99	19.45	0.57
SD	26	9.03	8.43	0.93	15.71	17.57	1.12	23.96	17.47	0.73
Qbs	49	5.98	6.41	1.07	29.65	11.21	0.38	61.04	33.97	0.56
Trgr	153	9.24	12.49	1.35	15.20	12.79	0.84	36.71	27.80	0.76
PE	67	7.05	12.95	1.84	20.26	32.36	1.60	46.45	140.53	3.03
PTrv/Ptru	131	8.53	11.65	1.37	41.54	22.71	0.55	45.11	20.01	0.44
Pv	6	7.67	2.66	0.35	108.50	27.29	0.25	69.83	10.03	0.14

The average values (X) of As in Upper Carboniferous (C2), Permian–Triassic mixed marine sedimentary rocks (PTr), and Early–Middle Permian Limestone Sa Kaeo Suture Melange (Ps-2) were 22.33 ppm, 19.74 ppm, and 19.74 ppm, respectively, which are higher than the average value of the whole unit, but the coefficient (CV) was low, showing weak activity, and rich in As. The coefficient of variation (CV) in Precambrian (PE), Jurassic Phu Kradung Formation (Jpk), and Early–Middle Permian Limestone (Ps-1) was 1.84 ppm, 1.82 ppm, and 1.78 ppm, respectively, and the Quaternary (Q) in the eastern part had the highest value of 2.15 ppm, which shows that the active migration ability of As is strong.

The average values (X) of Cu in Permian volcanic (Pv), Permian–Triassic volcanic (PTru, PTrv), Early–Middle Permian Limestone Sa Kaeo Suture Melange (Ps-2), and Devonian–Carboniferous (DC) were 108.50 ppm, 41.54 ppm, 31.12 ppm, and 30.39 ppm, respectively, which are higher than the average value of the whole unit, and the coefficient (CV) was low, where Permian volcanic (Pv) was the lowest, showing very weak activity and strong stability. The coefficient of variation (CV) in Precambrian (PE) and Silurian–Devonian (SD) was 1.60 ppm and 1.12 ppm, respectively, and the Quaternary (Q) in the eastern part had the highest value of 2.63, which shows that the active migration ability of Cu is strong.

Zn's average values (X) in Permian volcanic (Pv), basalt deposits (Qbs), and the Quaternary (Q) were 69.83 ppm, 61.04 ppm, and 57.38 ppm, respectively, which are higher than the average value of the whole unit, and the coefficient (CV) was low, where Permian volcanic (Pv) was the lowest, showing very weak activity and strong stability. The coefficient of variation (CV) in the Quaternary (Q) and Precambrian (PE) was 3.60 ppm and 3.03 ppm, respectively, which shows that the active migration ability of Zn is strong.

Comparing an element's concentration in a specific sample or location to its corresponding Clarke value [82] yields insights into whether that element's abundance deviates from the crustal average. As reference values, Earth's crust averages were around 1.5 ppm for As, 50 ppm for Cu, and 75 ppm for Zn [83]. To quantify this, we computed the concentration coefficient by dividing the elements' sample concentrations by their Clarke values, resulting in the following coefficients: As (4.70), Cu (0.40), and Zn (0.62). These

coefficients hold significant implications for mineralization. A coefficient greater than 1, as exemplified by As at 4.70, signifies enrichment compared to the crust, indicating geological processes potentially linked to gold mineralization. Conversely, coefficients be-low 1, such as Cu (0.40) and Zn (0.62), suggest depletion, implying a region less influ-enced by typical geology and mineralization processes associated with these elements.

4.3. Determining Thresholds Using the S-A Model

　　　The decomposed geochemical maps were produced by IDW using the S-A method, which was applied to each raster map: anomalies and backgrounds of the distributions for As, Cu, and Zn were built up using the inverse distance weighting (IDW) interpolation method [84], by ArcGIS software (Figure 6). One of the most widely used moving-average interpolation methods is IDW, which works under the concept that within-observations' values have more effect on interpolated values than distant observations' values. The IDW approach has the benefit of being easy to use and understand, and it is also simple to apply. The main issue is from the weights being determined solely based on location and ignoring the variance of the results [85]. The failure to consider the local features of data is a typical flaw in moving-average interpolation techniques such as IDW. Then, the power spectrum densities (S) were calculated for the elemental distributions. The S-A multifractal model was used to decompose complex geochemical patterns into constituent anomalous and background patterns [84], and it was implemented with the aid of GeoDAS software [34]. The power spectrum density (S) and the area (A) that is greater than or equal to S could be fitted with two straight lines using the least square method.

　　　The S-A plot, consisting of S versus the number of cells greater than or equal to S, could be fitted by three straight lines using the least square method. The three straight lines represent the geochemical noise, anomaly, and background, respectively [3]. Then, these three components were converted to the spatial domain by an inverse Fourier transformation. The decomposed maps show the spatial distribution of the geochemical anomaly and the geochemical background of As, Cu, and Zn.
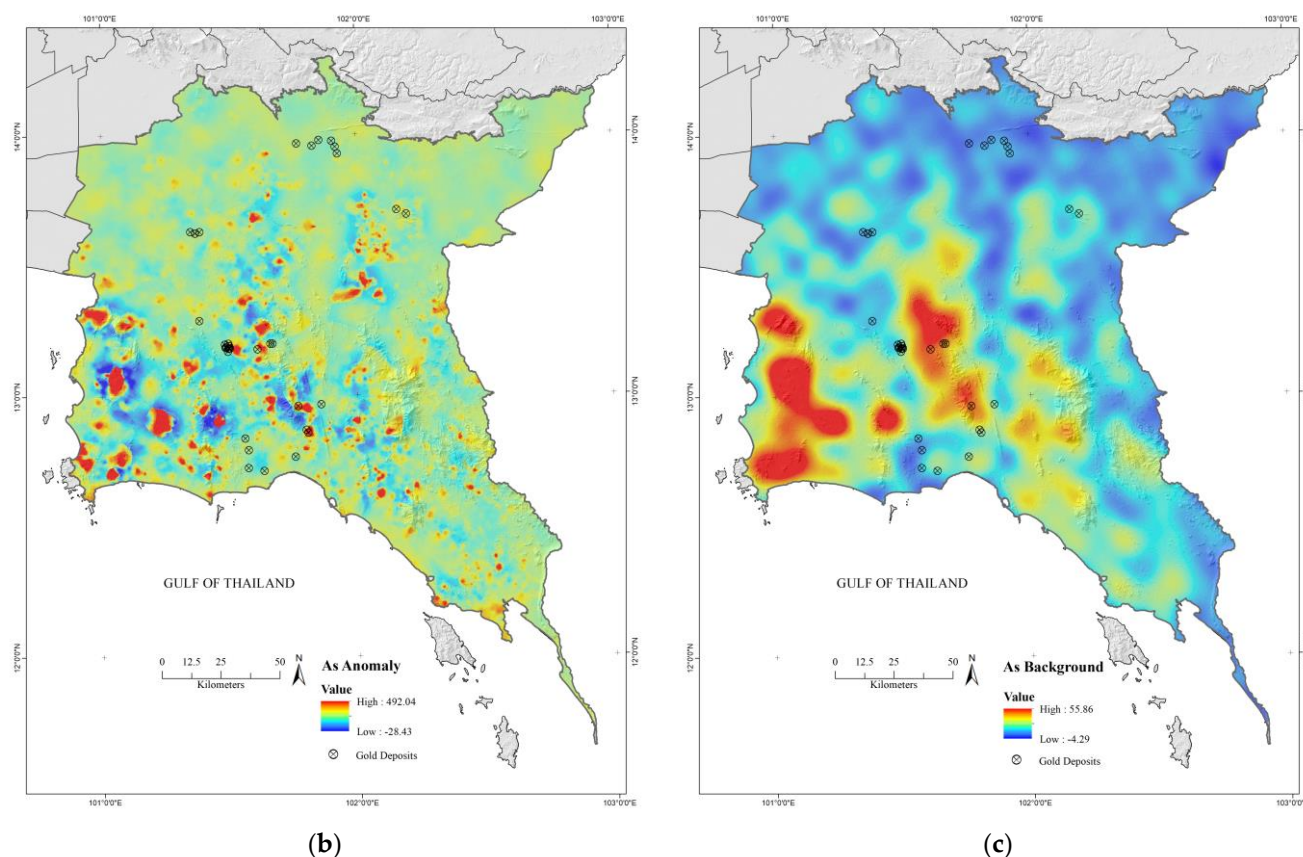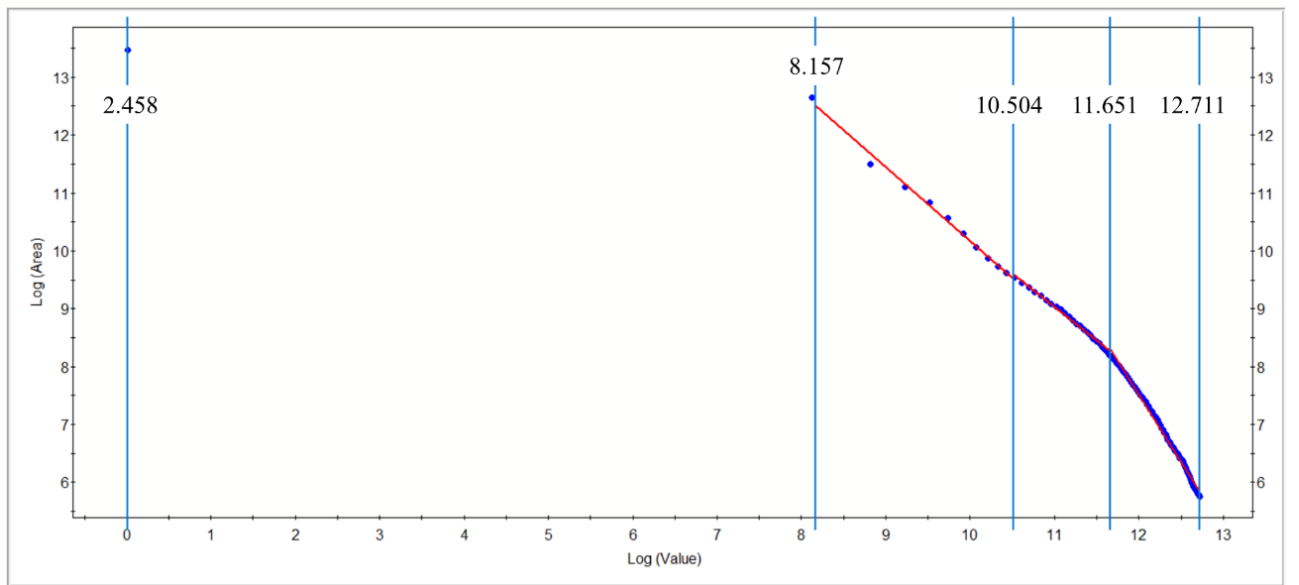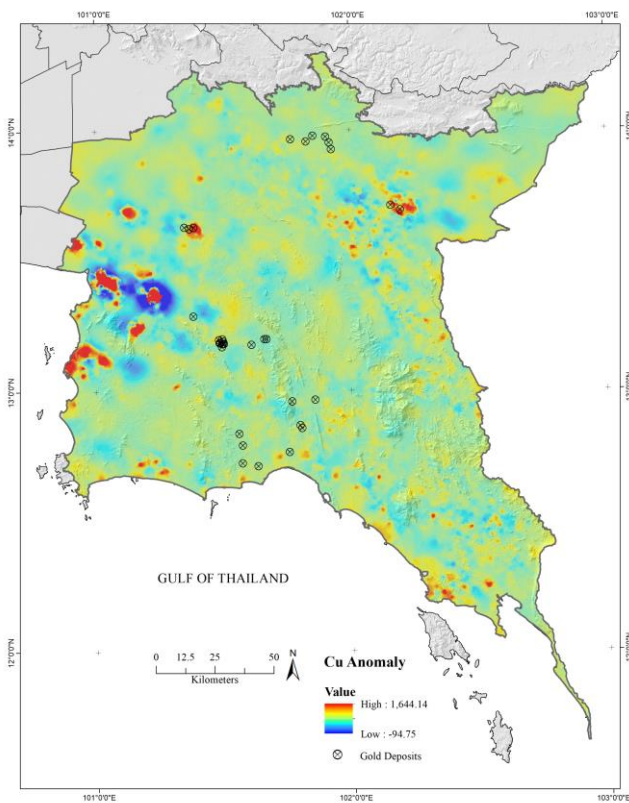

(**a**)

Figure 6. *Cont.*

(b)

(c)
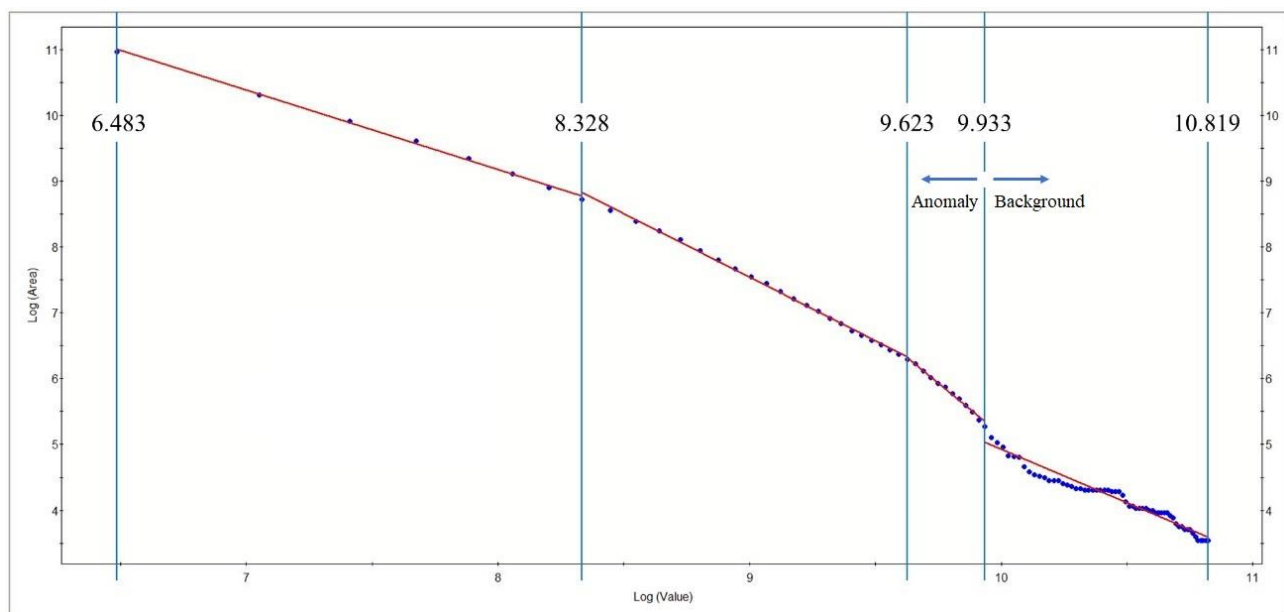
Figure 6. (**a**) Log–log plot of spectrum density (S) versus the number of cells greater than or equal to S (log base e) for As. (**b**) The decomposed map anomaly component of As. (**c**) The decomposed map background component of As.

Using the S-A approach, the geochemical map of As concentration (Figure 6) was divided into two spatial components. The As geochemical map was converted into the frequency domain using a Fourier transform. The relationship between A ($\geq$S) and S is shown on an As log–log scale (Figure 6a). The data can be fitted with three straight-line segments using the least squares method [86]. These segments represent three power energy spectrum ranges, each distinguished by a unique scaling property of the S–A relation. There are three ranges of S: left (S $\leq$ 4138), middle (4138 < S $\leq$ 20,606), and right (S $\geq$ 20,606). The last segment displays a short-range spectrum of high frequencies. Two filters were defined using two distinct ranges of S, separated by the threshold value S = 20,606: an anomaly filter with S < 20,606 (Figure 6b) and a background filter with S > 20,606 (Figure 6c). These filters are irregularly shaped to preserve the anisotropy and interior structure of the two-dimensional power energy spectrum, which they represent. The two maps are the result of applying the two filters obtained from the S-A plot to the Fourier-transformed functions, and then converting them back into the spatial domain.
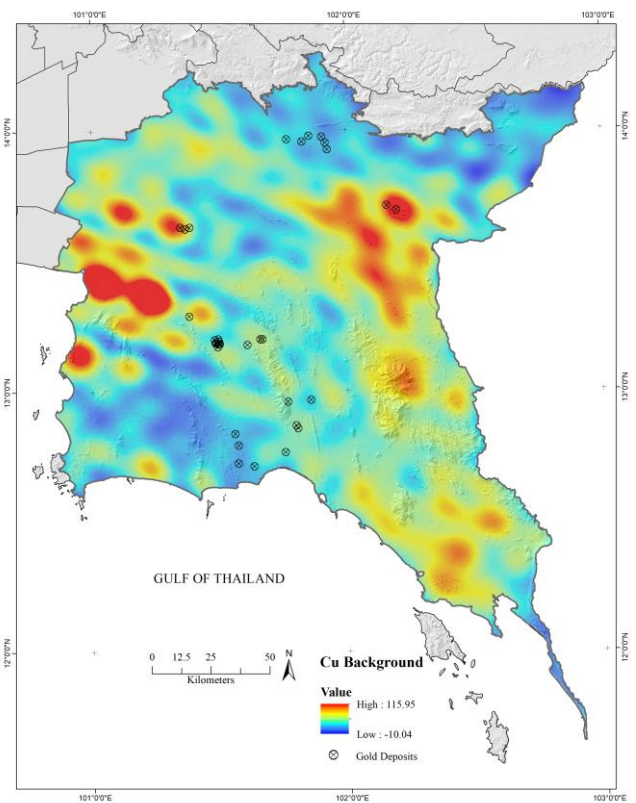
The geochemical map of Cu concentration (Figure 7) was decomposed into two spatial components using the S-A method. The Cu geochemical map was converted into the frequency domain using a Fourier transform. The relationship between A ($\geq$S) and S is shown on an As log–log scale (Figure 7a). There are three ranges of S: left (S $\leq$ 3488), middle (3488 < S $\leq$ 114,777), and right (S $\geq$ 114,777). The last segment displays a short-range spectrum of high frequencies. Two filters were defined using two distinct ranges of S, separated by the threshold value S = 114,777: an anomaly filter with S < 114,777 (Figure 7b) and a background filter with S > 114,777 (Figure 7c).
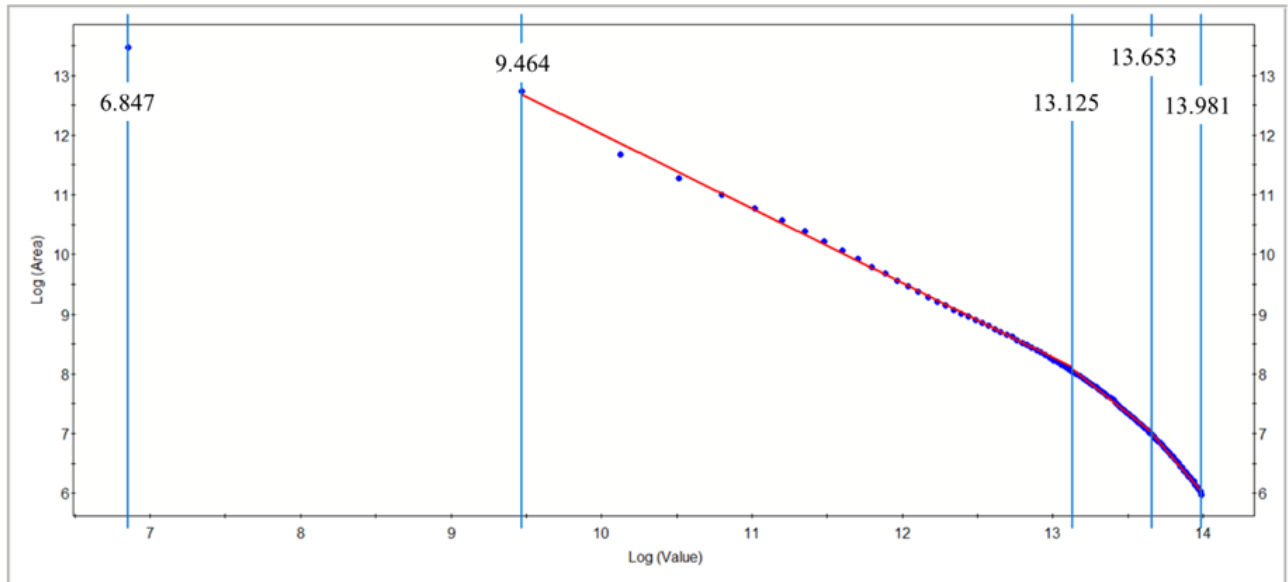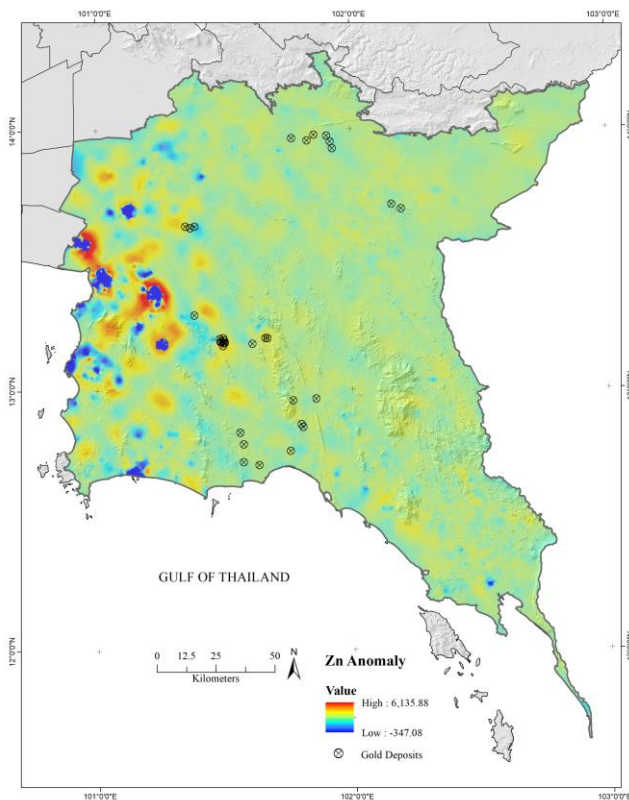
(**a**)

(**b**)

(**c**)

Figure 7. (**a**) Log–log plot of spectrum density (S) versus the number of cells greater than or equal to S (log base e) for Cu. (**b**) The decomposed map anomaly component of Cu. (**c**) The decomposed map background component of Cu.

The S-A approach was used to divide the geochemical map of Zn concentration (Figure 8) into two spatial components. Using a Fourier transform, the Zn geochemical map was transformed into the frequency domain. The relationship between A (≥S) and S is shown on an As log–log scale (Figure 8a). There are three ranges of S: left (S ≤ 12,889), middle (12,889 < S ≤ 850,339), and right (S ≥ 850,339). The last segment displays a short-
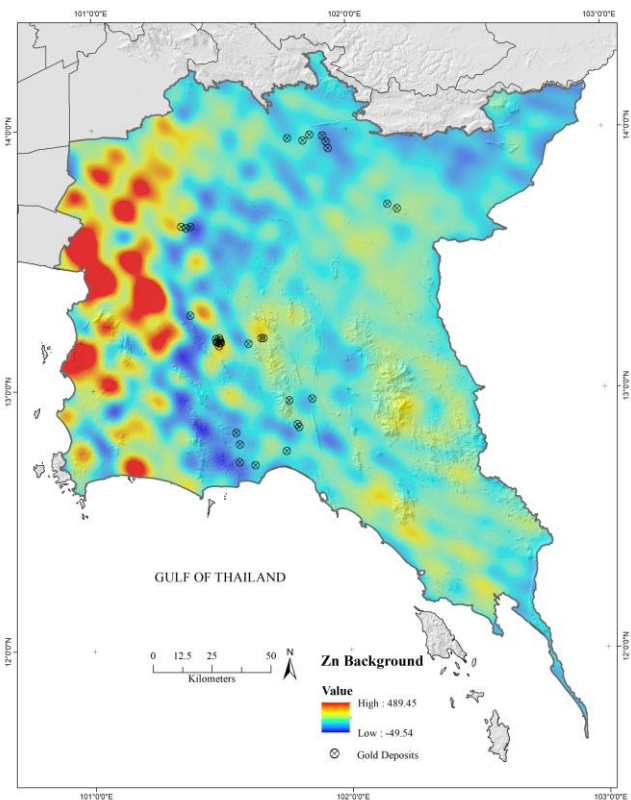
range spectrum of high frequencies. Two filters were defined using two distinct ranges of S, separated by the threshold value S = 850,339: an anomaly filter with S < 850,339 (Figure 8b) and a background filter with S > 850,339 (Figure 8c).

(**a**)

(**b**)   (**c**)

Figure 8. (**a**) Log–log plot of spectrum density (S) versus the number of cells greater than or equal to S (log base e) for Zn. (**b**) The decomposed map anomaly component of Zn. (**c**) The decomposed map background component of Zn.

The decomposed pattern obtained from the concentration map of arsenic (As) using the background filter revealed variations in As concentration values in the background, which could indicate favorable geological conditions for the occurrence of gold mineralization. Overlaying the known gold deposits on a background map shows that these deposits are located within areas characterized by high background As values found around intrusive and sedimentary rocks in the central (zone II) and eastern parts (zone III). The anomaly map suggests high mineral deposit potential in areas with NW–SE-trending faults and mapped intrusions [87]. Most of the As anomaly map shows that high values followed around intrusive rocks in the middle zone, Chanthaburi terrane, and along NW–SE-trending faults/fractures, which are favorable areas for mineral deposits. These results of the As element anomaly assessment of pathfinder elements for gold deposits may indicate the potential relationship with the gold deposits in the study area. The integrated anomalies of As occur around the intrusions and in the vicinity of faults in the center. However, the As anomalies occurring in the western part of the study area are not relative to gold deposits and may be caused by the high background concentration values of the intrusive rock of the Sibumasu terrane, which is divided by the tectonic line NW–SE trend. As anomaly assessment and pathfinder elements for gold deposits support this potential [88,89], and further investigation of gold anomalies around intrusions and faults is recommended.

Similar maps with distinctive features were generated using copper (Cu) and zinc (Zn) data. These two maps are also displayed in Figures 7 and 8, depicting the NE–SW distribution characteristics of the area. Interestingly, with the high concentrations observed in the geochemical maps of the study area, most of the anomalies did not align with the presence of the known gold deposits in the western part (zone I). Instead, they were primarily distributed in the western part around the intrusive and sedimentary rocks of the Sibumasu terrane. The central (zone II) showed that the high anomaly value followed around the Precambrian rocks (PE).

5. Conclusions

1. Stream sediment geochemical data analysis provides a robust means to identify potential mineral deposits across a large region. Traditional statistical methods may fail to account for spatial variability in complex geological settings, but incorporating the S-A multifractal model helps to better interpret the data. This approach provides an enhanced understanding of the geological processes, furthering our ability to pinpoint exploration targets. Through statistical analysis, this study uncovered a distinct distribution of elements such as As, Cu, and Zn across various geological units. These findings offer crucial insight into the dynamic interactions of elements within different geological contexts, revealing the migration abilities of these elements in specific units. Overall, the study demonstrated that the S-A multifractal model provides a powerful tool for analyzing stream sediment geochemical data. This approach helps to identify specific geological processes that contribute to patterns in the data, improving the understanding of statistical results and the regularity of changes in these properties in spatial and temporal domains. This information proves valuable in identifying precise exploration targets for mineral deposits.

2. By applying the S-A multifractal model and the inverse distance weighting (IDW) method, this research has successfully decomposed geochemical maps into anomalous and background patterns. The anomaly map for As, in particular, showed a strong correlation with the gold deposits in the study area, indicating its potential as a reliable indicator for identifying gold deposits. While geochemical maps derived from stream sediment data offer an initial understanding of element distribution, it is important to exercise caution during interpretation due to potential influences from regional geological factors.

3. Here, we created prediction maps, pinpointing areas of interest associated with pathfinder elements within the gold deposit zones and beyond. These maps can guide mineral exploration by narrowing down target areas for further investigation.

This study underlines the importance of utilizing a variety of analytical methods for accurate results, acknowledging that regional geological factors can contribute to elevated values unrelated to mineralization.

References

1. Cheng, Q. Singularity theory and methods for mapping geochemical anomalies caused by buried sources and for predicting undiscovered mineral deposits in covered areas. *J. Geochem. Explor.* **2012**, *122*, 55–70. [CrossRef]
2. Zuo, R.; Cheng, Q.; Xia, Q. Application of fractal models to characterization of vertical distribution of geochemical element concentration. *J. Geochem. Explor.* **2009**, *102*, 37–43. [CrossRef]
3. Cheng, Q. Mapping singularities with stream sediment geochemical data for prediction of undiscovered mineral deposits in Gejiu, Yunnan Province, China. *Ore Geol. Rev.* **2007**, *32*, 314–324. [CrossRef]
4. Parsa, M.; Maghsoudi, A.; Yousefi, M. A Receiver Operating Characteristics-Based Geochemical Data Fusion Technique for Targeting Undiscovered Mineral Deposits. *Nat. Resour. Res.* **2017**, *27*, 15–28. [CrossRef]
5. Zuo, R.; Xiong, Y. Geodata science and geochemical mapping. *J. Geochem. Explor.* **2019**, *209*, 106431. [CrossRef]
6. Grunsky, E.C.; de Caritat, P. State-of-the-art analysis of geochemical data for mineral exploration. *Geochem. Explor. Environ. Anal.* **2019**, *20*, 217–232. [CrossRef]
7. Zuo, R.; Wang, J.; Xiong, Y.; Wang, Z. The processing methods of geochemical exploration data: Past, present, and future. *Appl. Geochem.* **2021**, *132*, 105072. [CrossRef]
8. Cohen, D.; Kelley, D.; Anand, R.; Coker, W. Major advances in exploration geochemistry, 1998–2007. *Geochem. Explor. Environ. Anal.* **2010**, *10*, 3–16. [CrossRef]
9. Winterburn, P.A.; Noble, R.R.P.; Lawie, D. Advances in exploration geochemistry, 2007 to 2017 and beyond. *Geochem. Explor. Environ. Anal.* **2020**, *20*, 157–166. [CrossRef]
10. Zuo, R.; Carranza, E.J.M.; Cheng, Q. Fractal/multifractal modelling of geochemical exploration data. *J. Geochem. Explor.* **2012**, *122*, 1–3. [CrossRef]
11. Xie, S.; Wan, X.; Dong, J.; Wan, N.; Jiang, X.; Carranza, E.J.M.; Wang, X.; Chang, L.; Tian, Y. Quantitative prediction of potential areas likely to yield Se-rich and Cd-low rice using fuzzy weights-of-evidence method. *Sci. Total Environ.* **2023**, *889*, 164015. [CrossRef]
12. Yang, F.; Xie, S.; Hao, Z.; Carranza, E.J.M.; Song, Y.; Liu, Q.; Xu, R.; Nie, L.; Han, W.; Wang, C.; et al. Geochemical Quantitative Assessment of Mineral Resource Potential in the Da Hinggan Mountains in Inner Mongolia, China. *Minerals* **2022**, *12*, 434. [CrossRef]
13. Cohen, D.; Bowell, R. 13.24-Exploration geochemistry. In *Treatise on Geochemistry*, 2nd ed.; Holland, H.D., Turekian, K.K., Eds.; Elsevier: Amsterdam, The Netherlands, 2014; pp. 623–650.
14. Xie, S.; Huang, N.; Deng, J.; Wu, S.; Zhan, M.; Carranza, E.J.M.; Zhang, Y.; Meng, F. Quantitative prediction of prospectivity for Pb–Zn deposits in Guangxi (China) by back-propagation neural network and fuzzy weights-of-evidence modelling. *Geochem. Explor. Environ. Anal.* **2022**, *22*, geochem2021-085. [CrossRef]
15. Wang, W.; Xie, S.; Carranza, E.J.M. Introduction to the thematic collection: Applications of innovations in geochemical data analysis. *Geochem. Explor. Environ. Anal.* **2023**, *23*, geochem2022-058. [CrossRef]

16. Parsa, M.; Carranza, E.J.M. Modulating the Impacts of Stochastic Uncertainties Linked to Deposit Locations in Data-Driven Predictive Mapping of Mineral Prospectivity. *Nat. Resour. Res.* **2021**, *30*, 3081–3097. [CrossRef]
17. Chen, Y.; Sun, G.; Zhao, Q. Detection of multivariate geochemical anomalies associated with gold deposits by using distance anomaly factors. *J. Geochem. Explor.* **2020**, *221*, 106704. [CrossRef]
18. Xie, S.; Bao, Z. Fractal and Multifractal Properties of Geochemical Fields. *Math. Geol.* **2004**, *36*, 847–864. [CrossRef]
19. Carranza, E.J.M. *Geochemical Anomaly and Mineral Prospectivity Mapping in GIS.*; Elsevier: Amsterdam, The Netherlands, 2008.
20. Harris, D.; Pan, G. Mineral Favorability Mapping: A Comparison of Artificial Neural Networks, Logistic Regression, and Discriminant Analysis. *Nat. Resour. Res.* **1999**, *8*, 93–109. [CrossRef]
21. Harris, J.; Wilkinson, L.; Grunsky, E. Effective use and interpretation of lithogeochemical data in regional mineral exploration programs: Application of Geographic Information Systems (GIS) technology. *Ore Geol. Rev.* **2000**, *16*, 107–143. [CrossRef]
22. Hawkes, H.E.; Webb, J.S. *Geochemistry in Mineral Exploration*; Harper and Row: New York, NY, USA, 1962.
23. Sinclair, A. Selection of threshold values in geochemical data using probability graphs. *J. Geochem. Explor.* **1974**, *3*, 129–149. [CrossRef]
24. Tukey, J.W. *Exploratory Data Analysis*; Addison-Wesley: Reading, MA, USA, 1977; Volume 2.
25. Stanley, C.R.; Sinclair, A.J. Comparison of probability plots and the gap statistic in the selection of thresholds for exploration geochemistry data. *J. Geochem. Explor.* **1989**, *32*, 355–357. [CrossRef]
26. Matheron, G. *Traité de Géostatistique Appliquée, Mém BRGM 14*; Éditions Technip: Paris, France, 1962.
27. Mandelbrot, B.B. *The Fractal Geometry of Nature*; WH Freeman and Company: New York, NY, USA, 1983.
28. Turcotte, D.L. Fractals in geology and geophysics. *Pure Appl. Geophys.* **1989**, *131*, 171–196. [CrossRef]
29. Cheng, Q. Multifractality and spatial statistics. *Comput. Geosci.* **1999**, *25*, 949–961. [CrossRef]
30. Zhang, Y.; Ye, X.; Xie, S.; Zhou, X.; Awadelseid, S.F.; Yaisamut, O.; Meng, F. Implication of multifractal analysis for quantitative evaluation of mineral resources in the Central Kunlun area, Xinjiang, China. *Geochem. Explor. Environ. Anal.* **2022**, *22*, geochem2021-083. [CrossRef]
31. Cheng, Q.; Agterberg, F.; Ballantyne, S. The separation of geochemical anomalies from background by fractal methods. *J. Geochem. Explor.* **1994**, *51*, 109–130. [CrossRef]
32. Behera, S.; Panigrahi, M.K. Mineral prospectivity modelling using singularity mapping and multifractal analysis of stream sediment geochemical data from the auriferous Hutti-Maski schist belt, S. India. *Ore Geol. Rev.* **2021**, *131*, 104029. [CrossRef]
33. Cheng, Q. Spatial and scaling modelling for geochemical anomaly separation. *J. Geochem. Explor.* **1999**, *65*, 175–194. [CrossRef]
34. Cheng, Q. GeoData Analysis System (GeoDAS) for mineral exploration: User's guide and exercise manual. In Proceedings of the Material for the Training Workshop on GeoDAS Held at York University, Toronto, ON, Canada, 1–3 November 2000.
35. Koohzadi, F.; Afzal, P.; Jahani, D.; Pourkermani, M. Geochemical exploration for Li in regional scale utilizing Staged Factor Analysis (SFA) and Spectrum-Area (SA) fractal model in north central Iran. *Iran. J. Earth Sci.* **2021**, *13*, 299–307.
36. Sadeghi, B.; Agterberg, F. Singularity analysis. In *Encyclopedia of Mathematical Geosciences*; Springer: Cham, Switzerland, 2020; pp. 1–7.
37. Ali, K.; Cheng, Q.; Chen, Z. Multifractal power spectrum and singularity analysis for modelling stream sediment geochemical distribution patterns to identify anomalies related to gold mineralization in Yunnan Province, South China. *Geochem. Explor. Environ. Anal.* **2007**, *7*, 293–301. [CrossRef]
38. Cheng, Q. Multifractal interpolation method for spatial data with singularities. *J. S. Afr. Inst. Min. Met.* **2015**, *115*, 235–245. [CrossRef]
39. Zuo, R.; Wang, J. ArcFractal: An ArcGIS Add-In for Processing Geoscience Data Using Fractal/Multifractal Models. *Nat. Resour. Res.* **2020**, *29*, 3–12. [CrossRef]
40. Song, W.; Zheng, L.; Liu, J.; Cao, S.; Xie, Z. Genesis, metallogenic model, and prospecting prediction of the Nibao gold deposit in the Guizhou Province, China. *Acta Geochim.* **2023**, *42*, 136–152. [CrossRef]
41. Sunkari, E.D.; Appiah-Twum, M.; Lermi, A. Spatial distribution and trace element geochemistry of laterites in Kunche area: Implication for gold exploration targets in NW, Ghana. *J. Afr. Earth Sci.* **2019**, *158*, 103519. [CrossRef]
42. Agangi, A.; Reddy, S.M.; Plavsa, D.; Fougerouse, D.; Clark, C.; Roberts, M.; Johnson, T.E. Antimony in rutile as a pathfinder for orogenic gold deposits. *Ore Geol. Rev.* **2019**, *106*, 1–11. [CrossRef]
43. Bayari, E.E.; Foli, G.; Gawu, S.K.Y. Geochemical and pathfinder elements assessment in some mineralised regolith profiles in Bole-Nangodi gold belt in north-eastern Ghana. *Environ. Earth Sci.* **2019**, *78*, 268. [CrossRef]
44. Arhin, E.; Boadi, S.; Esoah, M.C. Identifying pathfinder elements from termite mound samples for gold exploration in regolith complex terrain of the Lawra belt, NW Ghana. *J. Afr. Earth Sci.* **2015**, *109*, 143–153. [CrossRef]
45. Anand, R.; Hough, R.; Salama, W.; Aspandiar, M.; Butt, C.; González-Álvarez, I.; Metelka, V. Gold and pathfinder elements in ferricrete gold deposits of the Yilgarn Craton of Western Australia: A review with new concepts. *Ore Geol. Rev.* **2019**, *104*, 294–355. [CrossRef]
46. Behera, S.; Panigrahi, M.K.; Pradhan, A. Identification of geochemical anomaly and gold potential mapping in the Sonakhan Greenstone belt, Central India: An integrated concentration-area fractal and fuzzy AHP approach. *Appl. Geochem.* **2019**, *107*, 45–57. [CrossRef]
47. Mvile, B.N.; Abu, M.; Kalimenze, J. Trace Elements Geochemistry of In Situ Regolith Materials and Their Implication on Gold Mineralization and Exploration Targeting, Dodoma Region, East Africa. *Min. Met. Explor.* **2021**, *38*, 2075–2087. [CrossRef]

48.　Moreley, C.K.; Charusiri, P.; Watkinson, I.M.; Ridd, M.; Barber, A.; Crow, M. Structural geology of Thailand during the Cenozoic. In *The Geology of Thailand*; Geological Society of London: London, UK, 2011. [CrossRef]

49.　Ridd, M.F.; Barber, A.J.; Crow, M.J. Introduction to the geology of Thailand. In *The Geology of Thailand*; Geological Society of London: London, UK, 2011. [CrossRef]

50.　Charusiri, P. Geotectonic evolution of Thailand: A new synthesis. *J. Geol. Soc. Thai.* **2002**, *1*, 1–20.

51.　Metcalfe, I.; Henderson, C.; Wakita, K. Lower Permian conodonts from Palaeo-Tethys Ocean Plate Stratigraphy in the Chiang Mai-Chiang Rai Suture Zone, northern Thailand. *Gondwana Res.* **2017**, *44*, 54–66. [CrossRef]

52.　Sone, M.; Metcalfe, I.; Chaodumrong, P. The Chanthaburi terrane of southeastern Thailand: Stratigraphic confirmation as a disrupted segment of the Sukhothai Arc. *J. Asian Earth Sci.* **2012**, *61*, 16–32. [CrossRef]

53.　Hara, H.; Tokiwa, T.; Kurihara, T.; Charoentitirat, T.; Ngamnithiporn, A.; Visetnat, K.; Tominaga, K.; Kamata, Y.; Ueno, K. Permian—Triassic back-arc basin development in response to Paleo-Tethys subduction, Sa Kaeo—Chanthaburi area in Southeastern Thailand. *Gondwana Res.* **2018**, *64*, 50–66. [CrossRef]

54.　Sone, M.; Metcalfe, I. Parallel Tethyan sutures and the Sukhothai Island-arc system in Thailand and beyond. In Proceedings of the International Symposia on Geoscience Resources and Environments of Asian Terranes (GREAT 2008), 4th IGCP 516 and 5th APSEG, Bangkok, Thailand, 24–26 November 2008.

55.　Saesaengseerung, D.; Agematsu, S.; Sashida, K.; Sardsud, A. Discovery of Lower Permian Radiolarian and Conodont Faunas from the Bedded Chert of the Chanthaburi Area Along the Sra Kaeo Suture Zone, Eastern Thailand. *Paleontol. Res.* **2009**, *13*, 119–138. [CrossRef]

56.　Fontaine, H.; Salyapongse, S. Unexpected discovery of early Carboniferous (late Visean-Serpukhovian) corals in East Thailand. In Proceedings of the International Conference on Stratigraphy and Tectonic Evolution of Southeast Asia and the South Pacific, Bangkok, Thailand, 19–24 August 1997.

57.　Fontaine, H.; Salyapongse, S.; Suteethorn, V.; Tansuwan, V.; Vachard, D. Recent biostratigraphic discoveries in Thailand: A preliminary report. *CCOP Newsl.* **1996**, *21*, 14–15.

58.　Fontaine, H.; Salyapongse, S.; Vachard, D. The Carboniferous of East Thailand—New information from microfossils. *Bull. Geol. Soc. Malays.* **1999**, *43*, 461–465. [CrossRef]

59.　Salyapongse, S. Geology of the Eastern Thailand, Field Excursion Guidebook Route no. 1. In Proceedings of the 1st International conference on Stratigraphy and Tectonic Evolution of Southeast Asia and the South Pacific, Bangkok, Thailand, 19–24 August 1997.

60.　Bunopas, S. *Palaeogeographic History of Western Thailand and Adjacent Parts of Southeast Asia. A Plate Tectonics Interpretation*; Geological Survey Division, Department of Mineral Resources: Bangkok, Thailand, 1982.

61.　Chaodumrong, P.; Salyapongse, S.; Sarapirome, S.; Palang, P. Geology of SW Khorat Plateau and eastern Thailand. In *Post-Symposium Excursion Guidebook of Symposium on Geology of Thailand*; Department of Mineral Resources Thailand: Bangkok, Thailand, 2002.

62.　Chutakositkanon, V.; Hisada, K.I.; Choowong, M.; Thitimakorn, T. Tectono-stratigraphy of the Sa Kaeo-Chanthaburi accretionary complex, Eastern Thailand: Reconstruction of tectonic evolution of oceanic plate-Indochina collision. In Proceedings of the International Symposia on Geoscience Resources and Environments of Asian Terranes (GREAT 2008), 4th IGCP 516 and 5th APSEG, Bangkok, Thailand, 24–26 November 2008.

63.　Crow, M. *Appendix. Radiometric Ages of Thailand Rocks*; The Geology of Thailand; Geological Society: London, UK, 2011; pp. 593–614.

64.　Metcalfe, I. *Palaeozoic–Mesozoic History of SE Asia*; Special Publications; Geological Society: London, UK, 2011; Volume 355, pp. 7–35.

65.　DMR. *Geologic Map of Thailand 1: 2,500,000: Geological Map of Thailand*; Geological Survey Division, Department of Mineral Resources: Bangkok, Thailand, 1999.

66.　Tansuwan, V. *Geological Map of Changwat Trat 1:250,000*; Department of Mineral Resources: Thailand, Bangkok, 1997.

67.　Tansuwan, V. *Geology and Mineral Resources Map of Changwat Chanthaburi 1:250,000*; Department of Mineral Resources: Bangkok, Thailand, 1997.

68.　Charusiri, P.; Pongsapitch, W.; Daorerk, V.; Charusiri, B. Anatomy of Chanthaburi granitoids: Geochronology, petrochemistry, tectonics, and associated mineralization. In Proceedings of the National Conference on Geologic Resources of Thailand: Potential for Future Development, Bangkok, Thailand, 17–24 November 1992; Department of Mineral Resources, Ministry of Industry: Bangkok, Thailand, 1992.

69.　Bunopas, S.; Vella, P. Tectonic and geologic evolution of Thailand. In Proceedings of the Workshop on Stratigraphic Correlation of Thailand and Malaysia, Bangkok, Thailand, 8–10 September 1983.

70.　Searle, M.P.; Whitehouse, M.J.; Robb, L.J.; Ghani, A.A.; Hutchison, C.S.; Sone, M.; Ng, S.W.-P.; Roselee, M.H.; Chung, S.-L.; Oliver, G.J.H. Tectonic evolution of the Sibumasu–Indochina terrane collision zone in Thailand and Malaysia: Constraints from new U–Pb zircon chronology of SE Asian tin granitoids. *J. Geol. Soc.* **2012**, *169*, 489–500. [CrossRef]

71.　Cobbing, E.J.; Mallick, D.I.J.; Pitfield, P.E.J.; Teoh, L.H. The granites of the Southeast Asian Tin Belt. *J. Geol. Soc.* **1986**, *143*, 537–550. [CrossRef]

72.　Brown, G.F. *Geologic Reconnaissance of the Mineral Deposits of Thailand*; US Government Printing Office: Washington, DC, USA, 1951.

73.　Searle, M.P.; Morley, C.K. Tectonic and thermal evolution of Thailand in the regional context of SE Asia. In *The Geology of Thailand*; Geological Society of London: London, UK, 2011; pp. 539–571. [CrossRef]

74. DMR. *Minerals Resources Map of Thailand 1:2,500,00*; Bureau of Mineral Resources, Department of Mineral Resources: Bangkok, Thailand, 2006.
75. Rose, A.; Hawkes, H.; Webb, J. *Geochemistry in Mineral Exploration*; Academic Press: London, UK, 1979.
76. Xie, S.; Cheng, Q.; Xing, X.; Bao, Z.; Chen, Z. Geochemical multifractal distribution patterns in sediments from ordered streams. *Geoderma* **2010**, *160*, 36–46. [CrossRef]
77. Van Loon, J.; Barefoot, R. *Analytical Methods for Geochemical Exploration*; Elsevier: Amsterdam, The Netherlands, 2013. [CrossRef]
78. Smith-Forbes, E.V.; Moore-Reed, S.D.; Westgate, P.M.; Ben Kibler, W.; Uhl, T.L. Descriptive analysis of common functional limitations identified by patients with shoulder pain. *J. Sport Rehabil.* **2015**, *24*, 179–188. [CrossRef]
79. Xu, Y.; Cheng, Q. A fractal filtering technique for processing regional geochemical maps for mineral exploration. *Geochem. Explor. Environ. Anal.* **2001**, *1*, 147–156. [CrossRef]
80. Zuo, R.; Wang, J. Fractal/multifractal modeling of geochemical data: A review. *J. Geochem. Explor.* **2016**, *164*, 33–41. [CrossRef]
81. Darnley, A.; Bjorklund, A.; Bolviken, B.; Gustaysson, N.; Koval, P. *A Global Geochemical Database. Recommendations for International Geochemical Mapping*; UNESCO: Paris, France, 1995.
82. Clarke, F.W.; Washington, H.S. *The Composition of the Earth's Crust*; US Government Printing Office: Washington, DC, USA, 1924; Volume 127.
83. Wedepohl, K.H. The composition of the continental crust. *Geochim. Cosmochim. Acta* **1995**, *59*, 1217–1232. [CrossRef]
84. Ghezelbash, R.; Maghsoudi, A.; Daviran, M. Combination of multifractal geostatistical interpolation and spectrum–area (S–A) fractal model for Cu–Au geochemical prospects in Feizabad district, NE Iran. *Arab. J. Geosci.* **2019**, *12*, 152. [CrossRef]
85. Xie, X.; Wang, X.; Zhang, Q.; Zhou, G.; Cheng, H.; Liu, D.; Cheng, Z.; Xu, S. Multi-scale geochemical mapping in China. *Geochem. Explor. Environ. Anal.* **2008**, *8*, 333–341. [CrossRef]
86. Ke, X.; Xie, S.; Zheng, Y.; Awadelseid, S.F.; Gao, S.; Tian, L. Multifractal analysis of geochemical stream sediment data in Bange region, northern Tibet. *J. Earth Sci.* **2015**, *26*, 317–327. [CrossRef]
87. Feng, L.; Yang, L.; Carranza, E.J.M.; Zeng, Y.; Le, X.; Zhang, Q.; Lu, J.; Xiao, C.; Huang, S.; Wang, Q. Mapping of geological complexity and analyzing its relationship with the distribution of gold deposits in the Guangxi Gold Ore Province, Southern China. *J. Geochem. Explor.* **2023**, *251*, 107238. [CrossRef]
88. Wu, R.; Chen, J.; Zhao, J.; Chen, J.; Chen, S. Identifying geochemical anomalies associated with gold mineralization using factor analysis and spectrum–area multifractal model in Laowan District, Qinling-Dabie Metallogenic Belt, Central China. *Minerals* **2020**, *10*, 229. [CrossRef]
89. Farahmandfar, Z.; Jafari, M.; Afzal, P.; Ardalan, A.A. Description of gold and copper anomalies using fractal and stepwise factor analysis according to stream sediments in NW Iran. *Geopersia* **2019**, *10*, 135–148. [CrossRef]